Materials Research Bulletin 122 (2020) 110691

Contents lists available at ScienceDirect

Materials Research Bulletin

journal homepage: www.elsevier.com/locate/matresbu

Fast, low-pressure, low-temperature microwave synthesis of ABW cesium aluminosilicate zeolite nanocatalyst in organotemplate-free hydrogel system

Tamara Mahmoud Ali Ghrear[a], Ying-Wai Cheong[a], Gin Keat Lim[a], Daniel Chateigner[b], Tau Chuan Ling[c], Soon Huat Tan[d], Eng-Poh Ng[a,*]

[a] School of Chemical Sciences, Universiti Sains Malaysia, 11800 USM Penang, Malaysia
[b] Normandie Université, CRISMAT-ENSICAEN and IUT-Caen, Université de Caen Normandie, 14050 Caen, France
[c] Institute of Biological Sciences, Faculty of Science, University of Malaya, 50603 Kuala Lumpur, Malaysia
[d] School of Chemical Engineering, Engineering Campus, Universiti Sains Malaysia, Penang, Malaysia

ARTICLE INFO

Keywords:
Sol-gel chemistry
Microporous materials
Crystal growth
Crystal structure
Catalytic properties

ABSTRACT

Cs-ABW zeolite nanocrystals were synthesized using a microwave-assisted hydrothermal technique without an organic template. Using powder X-ray diffraction Rietveld refinement and spectroscopy, we found that pure ABW-type $CsAlSiO_4$ zeolite nanocrystals (Si/Al ratio = 1.08) with an orthorhombic structure (space group *Pc21n*, a = 9.4425(21) Å; b = 5.4437(11) Å; c = 8.9152(19) Å) can be crystallized from a clear precursor solution of $4SiO_2$:$1Al_2O_3$:$16Cs_2O$:$160H_2O$ (180 °C, 6 min). The Cs-ABW nanoparticles had a mean particle size of 68 nm and were thermally and colloidally stable. The nanocrystals—which had high accessible basic sites, $(Si–O–Al)^-Cs^+$, located at their external surface—were active in catalyzing the cyanoethylation of aliphatic alcohols under non-microwave instant heating, with 100 % selectivity to the desired product and high catalyst reusability. Furthermore, the cyanoethylation of methanol catalyzed by nanocrystalline Cs-ABW under instant heating had equal or better reactivity than those catalyzed by other solid base catalysts.

1. Introduction

Zeolites are crystalline aluminosilicates with well-defined channels and cavities. Zeolites are commonly used in ion exchange, catalysis, and separation due to their unique crystalline structure and tunable surface properties [1,2]. Dividing zeolites into fine particles (< 100 nm) creates immense external surface area and affects their magnetic, optical, electrical, and catalytic properties [3–5], enabling structures with unique properties. Thus, the application of zeolites is expanding toward atomic energy, food, paper, drug delivery, ceramics, paints, electronics, recording materials, lubricants, detergents, and so on [6–10]. Among the 245 zeolite structures recognized to date, only the following frameworks can be synthesized at the nanometer scale: ANA [11], *BEA [12], EDI [13], EMT [14], FAU [15], GIS [16], LTA [17], LTJ [18], LTL [19], MEL [20], MER [21], MFI [22], MOR [23], SOD [24], AEI [25], AFI [26], AFO [27], and CHA [28].

Synthesizing zeolite nanocrystals involves hydrothermal treatment, using harmful organic additives as templates to control the crystal size of the zeolite [29–31]. Nanoscale zeolites can also be crystallized in sodium- and potassium-rich systems where the alkali metal cations can function as less toxic inorganic templates [14,18,21,32].

Cesium aluminosilicate zeolites are in high demand due to their strong base properties. However, the synthesis of Cs-zeolites is barely reported because doing so is tedious and dangerous, which requires high temperature (700–1200 °C), high pressure (> 1000 bar), and long crystallization time (46 h); also, nanoscale Cs-zeolite has not yet been reported [33–37]. The first work describing the characterization of pure Cs-aluminosilicate with ABW topology (eight-membered ring and one-dimensional pore channel, 3.4 × 3.8 $Å^2$) was reported in the 1970s [35]. Synthetic Cs-zeolite is interesting because it can be used in many applications such as heterogeneous basic solid catalysts [38] and hosts for immobilization of radioactive cesium [39–41]. The synthesis of Cs-zeolite would benefit from milder, safer synthesis conditions with lower heating temperature and pressure, so in this study we synthesize organotemplate-free nanoscale ABW-type Cs-zeolite using a more efficient microwave heating technique.

2. Experimental

2.1. Synthesis of ABW-type Cs-zeolite nanocrystals

Nanocrystalline ABW-type Cs-zeolite was prepared with a molar

* Corresponding author.
E-mail address: epng@usm.my (E.-P. Ng).

https://doi.org/10.1016/j.materresbull.2019.110691
Received 23 July 2018; Received in revised form 24 October 2019; Accepted 12 November 2019
Available online 12 November 2019

composition of $4SiO_2$:$1Al_2O_3$:$16Cs_2O$:$164H_2O$. Typically, a clear aluminate solution was prepared by dissolving a $CsOH{\cdot}H_2O$ pellet (10.500 g, 99.5 %; Sigma-Aldrich) and $Al(OH)_3$ (1.242 g, 99.9 %; Acros) in distilled water (8.063 g) at 110 °C for 24 h under continuous stirring. A clear silicate solution was prepared by mixing HS-40 (4.781 g, 40 % SiO_2, 60 % H_2O; Sigma-Aldrich) and $CsOH{\cdot}H_2O$ powder (32.2875 g) in distilled water (7.988 g), followed by stirring at room temperature for 10 min. Both solutions were then cooled to room temperature. The aluminate solution was slowly added to the silicate solution under vigorous stirring (15 min) until a clear precursor solution was obtained. The hydrogel was then placed in a 100-mL PTFE reaction vessel and capped, then subjected to microwave radiation at 180 °C by a microwave reactor (Anton Paar's Multiwave 3000) using 800 W power. The solid products were purified with distilled water and then freeze-dried. The samples are denoted as MW-*n*m, where *n* is the heating time in minutes.

2.2. Characterization

X-ray diffraction (XRD) patterns were recorded using a Bruker-AXS D8 X-ray diffractometer, and Rietveld refinement was performed with GSAS software. Field-emission scanning electron microscopy (FESEM) and transmission electron microscopy (TEM) were performed with JEOL JSM-6701F and Philips CM12 electron microscopes operated at 20 kV and 200 kV, respectively. The chemical compositions of zeolite were determined using a Philips PW2404 X-ray fluorescence (XRF) spectrometer. An infrared (IR) spectrum was recorded on a Perkin Elmer Spectrum One spectrometer using the KBr pellet technique (KBr:sample ratio = 50:1). Dynamic light scattering (DLS) and zeta potential (ζ) analyses were done using a Malvern Zetasizer Nano Series. Porosity analysis was performed using a Micromeritics ASAP 2010. Thermogravimetry/derivative thermogravimetry (TGA/DTG) results were measured using a Mettler TGA SDTA851.

2.3. Catalytic activity study

The cyanoethylation reaction was conducted as follows: Activated nanocrystalline Cs-ABW zeolite (0.500 g), alcohol (76 mmol, methanol, 99.5 %; ethanol, 99.9 %; propanol, 99.0 %; butanol, 99.0 %; cyclohexanol, 99.0 %; phenol, 99.0 %; benzyl alcohol, 99.0 %; Merck) and acrylonitrile (19 mmol, 99 %; Merck) were added to a 10-mL quartz vial. The vial was tightly capped, heated, and magnetically stirred (800 rpm) in an instant heating reactor (Anton Paar's Monowave 50). The reaction solution was withdrawn, and the zeolite catalyst was separated. The reaction products were evaluated with a GC-FID chromatograph (Agilent/HP 6890 GC, HP-5 capillary column) and a GC–MS (Perkin-Elmer Clarus 500).

3. Results and discussion

The formation of Cs-ABW nanozeolites was first characterized using powder XRD, as shown in Fig. 1. After 2 min of microwave heating, a broad band appeared at $2\theta = 27.5°$, implying that the MW-2 m sample was an amorphous solid (Fig. 1A(a)). After 5 min of hydrothermal heating, the amorphous hump slowly disappeared and several diffraction peaks started to appear at $2\theta = 18.80°$ [200/110], 27.52° [202/112], and 32.90° [310/020], indicating the formation of the ABW crystalline phase in the MW-4 m sample (Fig. 1A(b)). Heating the precursor solution for 6 min produced crystalline Cs-ABW zeolite with no competing crystalline phases (Fig. 1A(c)). The synthesis time for crystallizing the ABW zeolite framework was shorter and the pressure during the hydrothermal process was lower (20.5 bar) in this work than in previous works (46 h, > 1000 bar at 700–1200 °C) because the microwave electromagnetic radiation induced fast heating and high content of CsOH provided high alkalinity in precursor solution [13,34]. The XRD peaks of the Cs-ABW nanozeolite were intense and broad, due to its small crystallite size [26].

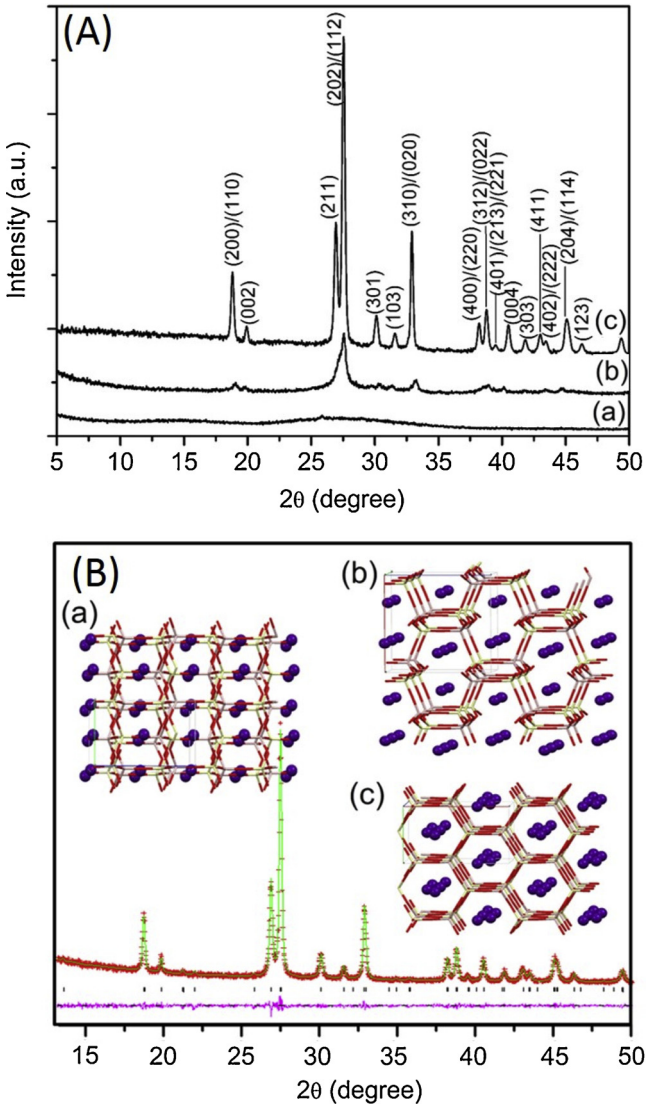

Fig. 1. (A) XRD patterns of (a) MW-2 m, (b) MW-5 m and (c) MW-6 m solids, and (B) Rietveld refinement of the XRD pattern of ABW-type Cs-zeolite (MW-6 m). Observed (solid line) and calculated (+ marks) XRD patterns, as well as the difference profile (bottom) are shown. Tick marks indicate peak positions. Inset: Crystal structure views along (a) *a*-direction (pore opening 8.23 × 4.39 $Å^2$), (b) *b*-direction (pore opening 8.23 × 4.39 $Å^2$) and (c) *c*-direction (pore opening 5.44 × 6.40 $Å^2$). Unit-cell is boxed. Purple: Cs, yellow: Si, pink: Al and red: O. (For interpretation of the references to colour in this figure legend, the reader is referred to the web version of this article).

The XRD pattern of Cs-ABW nanozeolite (MW-6 m) was indexed using the TREOR indexing program, and the crystallographic data are shown in Tables S1 and S2 (see Supporting Information). Table 1 lists the unit cell parameters of MW-6 m estimated using Rietveld refinements, compared with reported values [34]. Profile fitting with Rietveld refinement gave a quality fit (Fig. 1B), and all of the computed structural parameters agree with reported values. The Cs-ABW structure had a $Pc2_1n$ space group and lattice parameters of $a = 9.4432(9)$ Å, $b = 5.4441(4)$ Å, $c = 8.9158(7)$ Å, and $V = 458.36(10)$ $Å^3$. All the peaks were attributed to this structure, so this model accounts for pure synthesized Cs-ABW nanozeolite. The fit quality was also demonstrated by the low *R*-expected (R_{exp}), *R*-unweighted (R_p), and *R*-weighted pattern (R_{wp}) reliability factors as well as a goodness-of-fit (χ^2) close to 1 (Table 1) [42].

The coordinates of the Cs^+ extraframework cations, Al, Si, and O

Table 1
Crystallographic data of CsABW zeolites.

	Published*	Current work
Crystallite size	200 × 120 × 60 (μm^3)	70 × 50 × 6 (nm^3)
Data collection		
X-ray facility	Oxford Diffraction Xcalibur	PANalytical X'Pert PRO
X-ray radiation	Mo K_α	Cu K_α
Wavelength (Å)	0.70926	1.5406
Scan type	ω/φ	2θ
2θ range (°2θ)	3.000–62.000	5.000–50.000
Step size (°)	0.5	0.02
Unit cell		
Space group	$Pc2_1n$ (Orthorhombic)	$Pc2_1n$ (Orthorhombic)
a (Å)	9.414(1)	9.4432(9)
b (Å)	5.435(1)	5.4441(4)
c (Å)	8.875(1)	8.9158(7)
α (deg)	90	90
β (deg)	90	90
γ (deg)	90	90
V ($Å^3$)	457.9(4)	458.36(10)
Chemical composition		
Refined structure	[Cs]–[$SiAlO_4$]·xH_2O	[Cs]–[$SiAlO_4$]·yH_2O
Si/Al ratio	1.00	1.00
Rietveld refinement		
No. observations	n.d.#	1798
No. geometric restraints	n.d.#	0
No. structural parameters	n.d.#	49
No. profile parameters	n.d.#	11
$R_p = [\Sigma (y^{obs}-y^{calc})^2/\Sigma w(y^{obs})^2]^{1/2}$	n.d.#	0.0610
$R_{exp} = [(N-P + C)/\Sigma w_i(y_i^{obs})^2]^{1/2}$	n.d.#	0.0764
$R_{wp} = [\Sigma w_i(y^{obs}-y^{calc})^2/\Sigma w(y^{obs})^2]^{1/2}$	n.d.#	0.0817
$\chi^2 = (R_{wp}/R_{exp})^2$	n.d.#	1.143

* Reference [34].
\# n.d. = not determined.

atoms in the ABW structure framework were refined, and its crystal structure was viewed along the *a*-, *b*- and *c*-directions (inset of Fig. 1B). The ABW framework consisted of eight-membered ring (8MR) pore channels running along the [010] direction (inset of Fig. 1B(b)), where the Cs extraframework cations were merely located at the center of the 8MR channels and 6MR voids. All these results agree with the crystal structure proposed by Gatta et al. [34], determined by single-crystal XRD.

Fig. 2a shows an FESEM image of the Cs-ABW nanozeolite, revealing that the nanocrystals were discrete and showed no agglomeration. DLS analysis revealed a Cs-ABW nanozeolite with a narrow particle size distribution, which agrees with the FESEM analysis. The nanocrystals had a size range of 45–88 nm with an average hydrodynamic size of ~68 nm. The nanocrystals showed a zeta value of –52.6 mV, and they showed no sedimentation in water for over a month, demonstrating their long-term stability in colloidal form. Such nanocrystals, with high dispersibility and colloidal stability, are useful in advanced applications such as sensors, atomic energy production, ceramics, paints, electronics, recording materials, lubricants, and detergents. [3]. A TEM image of nanoscale Cs-ABW zeolite is also shown (inset of Fig. 2b), revealing oval crystals with an average crystallite size of 70 nm and it agrees with DLS analysis. Unlike conventional hydrothermal heating, which involves external heating, microwave irradiation heats the alkaline sol mixture internally, directly, and evenly [43–45], thus enhancing the solubilization of zeolite precursors in the alkaline medium. Such unique heating could enhance the supersaturation condition where zeolite nucleation is preferable to crystal growth, helping to form Cs-ABW zeolite nanocrystals that are smaller and more uniform [21].

Fig. 3 shows EDX analysis, with elemental maps of Cs-ABW nanozeolite revealing the Si, Al, O, Cs atoms and overlay localization. Interestingly, these four elements were abundant and evenly distributed among all granules. Quantitative XRF spectroscopy (Table 2) indicates that Cs had the highest weight percentage due to its heavy atomic weight. The Si/Al ratio was 1.08, while the Cs/Al ratio was 1.02. Thus, the synthesized nanocrystalline Cs-ABW had a composition of $Cs_{1.102}Al_{1.080}Si_{1.000}O_{4.017}$, which is close to the stoichiometric formula of its conventional counterpart, $CsAlSiO_4$ (Table 1) [34].

Fig. 4 shows an IR spectrum of the nanocrystalline Cs-ABW zeolite. The IR bands at 3465 and 1665 cm^{-1} were attributed to the stretching and bending modes of O—H groups of adsorbed water and silanol, respectively [46]. The strong bands at 1130, 1062, 986, and 449 cm^{-1} were attributed to the vibrational frequencies of the T—O—Si bonds (T = Si, Al) [47]. The IR bands at 541, 608, and 671 cm^{-1} were characteristics of the double zigzag chain (dzc) in the ABW zeolite. Also, the weak shoulder band at 859 cm^{-1} was attributed to the bending vibration of the free surface silanol (Si—OH) groups of zeolite [48].

Fig. 5a shows TG/DTG curves of the Cs-ABW (MW-6 m) nanocrystals. The first stage of weight loss (0.26 %) below 160 °C with an endothermic signal came from the release of physisorbed water [49,50]. The next stage of endothermal weight loss (0.75 %) below 400 °C was originated from desorption of chemisorbed water from the external surface of zeolite, and the weight loss (0.49 %) above 400 °C came from dehydroxylation (condensation) of silanol groups [48]. After combustion at 900 °C, ~98.5 % of the sample remained as an unburned solid, and the ABW crystal structure did not collapse even at 900 °C.

The TG/DTG results were further supported by an N_2 adsorption isotherm, where the nanoscale Cs-ABW zeolite exhibited a Type V adsorption-desorption isotherm (Fig. 5b). Furthermore, a type H3

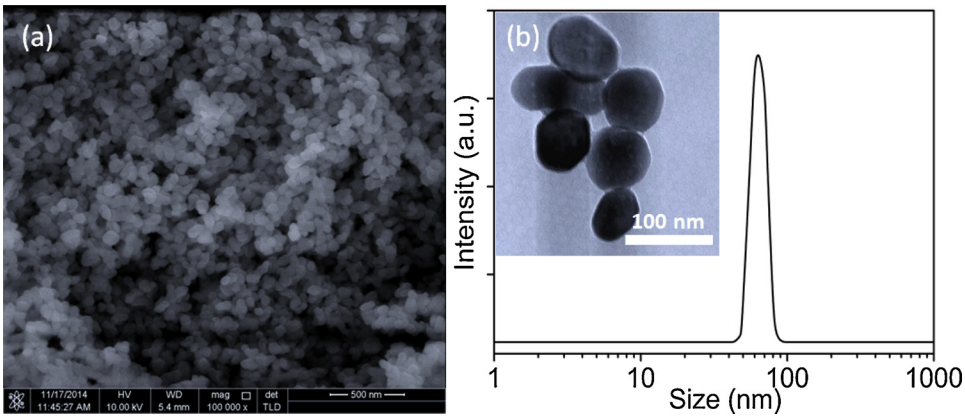

Fig. 2. (a) SEM image and (b) DLS plot of nanoscale Cs-ABW (MW-6 m). Inset of (b) shows the TEM image of Cs-ABW zeolite nanocrystals.

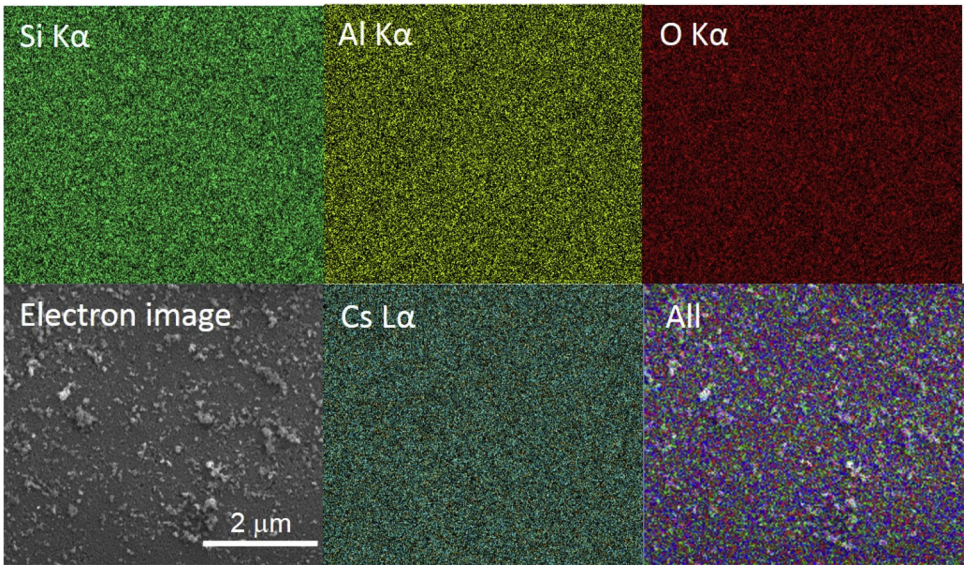

Fig. 3. Element distribution map (SEM/EDX) of nanoscale Cs-ABW (MW-6 m).

hysteresis loop appeared at high P/P_o due to the close packing of nanocrystals. An external surface area of 25 m^2/g and a total pore volume of 0.11 cm^3/g were measured. No microporosity appeared because the pores were blocked by the Cs^+ extraframework cations (inset of Fig. 1B). Nevertheless, this nanocrystalline material can be used as a solid catalyst because its external surface has highly accessible basic sites, $(Si{-}O{-}Al)^{-}Cs^{+}$.

To demonstrate this, we performed a model cyanoethylation reaction between acrylonitrile and various alcohols to study the potential of the Cs-ABW zeolite nanocrystals as a solid base catalyst. Without the zeolite catalyst, none of the alcohols showed conversion, even after 2 h. In contrast, the superior catalytic performance of Cs-ABW nanozeolite was clearly demonstrated as acrylonitrile reacting with aliphatic alcohols (acid-strengthening, high pKa) showed high conversion and high selectivity (100 %) within 30 min at 60 °C (Table 2), revealing that the cyanoethylation reaction was an activated catalytic reaction.

However, the conversion decreased as the carbon chain length of the alcohols increased, though the pKa values were almost identical

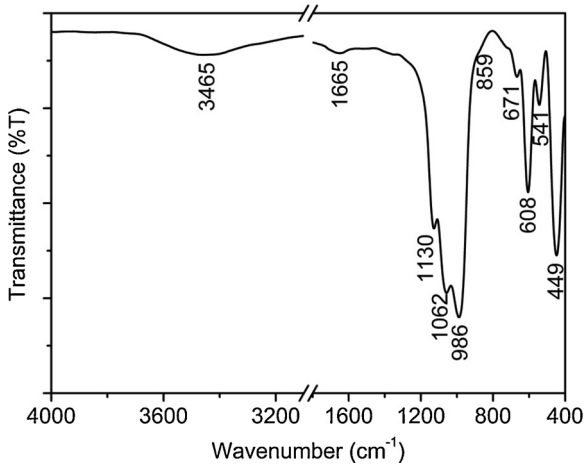

Fig. 4. FTIR spectrum of nanoscale Cs-ABW solid (MW-6 m).

Table 2
Cyanoethylation of alcohols with acrylonitrile catalyzed by nanocrystalline Cs-ABW zeolite.[a]

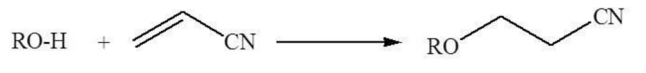

Alcohol Acrylonitrile 3-Alkoxypropanenitrile

Entry	Alcohols	Conversion (%)				T (°C)
		pKa value[e]	10 min	20 min	30 min	
1	Methanol	15.3	95.12	100	100	60
2	Methanol[b]	15.3	95.04	100	100	60
3	Ethanol	15.9	77.64	89.02	92.16	60
4	Propanol	16.1	41.57	61.96	72.55	60
5	Propanol[c]	16.1	22.74	38.58	49.60	60
6	Propanol	16.1	98.47	100	100	100
7	Butanol	16.1	92.94	96.86	98.18	100
8	Butanol[d]	16.1	92.91	96.57	97.75	160
9	Cyclohexanol	16.0	0	0	0	160
10	Phenol	10.0	4.71	7.84	10.59	160
11	Benzyl alcohol	15.4	0	0	0	160

[a] Reaction conditions: Cs-ABW (MW-6 m, 0.50 g), alcohol (76 mmol), acrylonitrile (19 mmol).
[b] 5th run of Entry 1; [c]oil bath heating (autoclave).
[d] 3rd run of Entry 6.
[e] ref. [51].

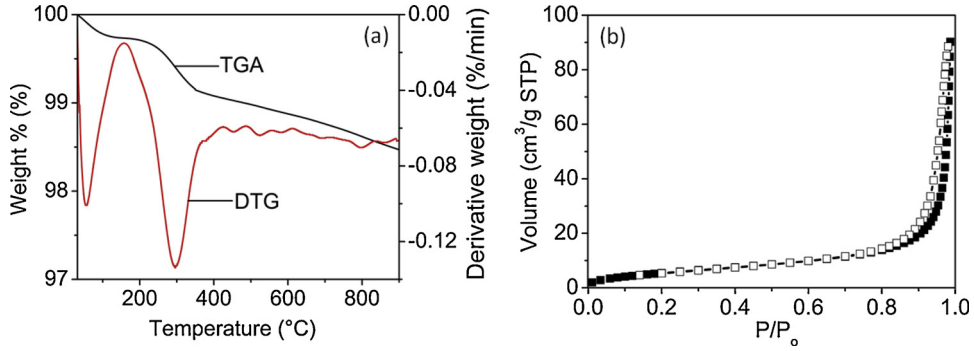

Fig. 5. (a) TG/DTG curves and (b) nitrogen gas adsorption (close symbols) and desorption (open symbols) isotherms of nanoscale Cs-ABW zeolite (MW-6 m).

Table 3
Comparative catalytic performance of nanoscale Cs-ABW with other reported catalysts on cyanoethylation of methanol reaction.

Catalyst	Conversion (%)	t (min)	T (°C)	Heating mode	Ref.
Nanosized Cs-ABW	100.0	20	60	Instant heating	Present work
MgO	98.7	120	50	Reflux	[52]
$Mg(OH)_2$	62.4	120	50	Reflux	[52]
CaO	94.7	120	50	Reflux	[52]
$Ca(OH)_2$	30.6	120	50	Reflux	[52]
SrO	98.9	120	50	Reflux	[52]
BaO	78.2	120	50	Reflux	[52]
KOH/alumina	85.3	120	50	Reflux	[52]
KF/alumina	52.3	120	50	Reflux	[52]
Mg-Al hydrotalcite	98.0	90	50	Reflux	[53]
Mg-Al-O-Bu^t-hydrotalcite	92.0	36	25	Reflux	[54]
Zeolite NaA	85.4	720	150	Autoclave	[55]
Zeolite NaA	48.7	720	150	Reflux	[55]
Zeolite MgO/Cs,N[a]Y	98.0	15	–[a]	Microwave	[56]
LiNKX-2	14.0	840	150	Autoclave	[57]
NaNKX-2	58.9	840	150	Autoclave	[57]
KNKX-2	69.2	840	150	Autoclave	[57]
CsNKX-2	89.9	840	150	Autoclave	[57]

[a] Not stated.

(Entries 1, 3, 4, 6, and 7). Furthermore, little to no conversion appeared when bulk molecules of cyclic alcohols (cyclohexanol, phenol, and benzyl alcohol) were used (Entries 9–11). We also compared heating methods—non-microwave instant heating *versus* oil bath heating (loaded in autoclave)—in the cyanoethylation of propanol (60 °C, 30 min). The first method showed a higher reaction conversion (72.55 %) (Entry 4) than the second one (49.60 %) (Entry 5). We also tested the reusability of the solid catalyst, finding that its conversion efficiency barely decreased and demonstrating its high recyclability (Entries 2 and 8).

The catalytic performance of the Cs-ABW nanozeolite was also compared with related catalysts in the cyanoethylation of methanol (Table 3) [52–57]. The reaction catalyzed by the Cs-ABW nanocatalyst under instant heating (100 %) showed more conversion the reactions catalyzed by other solid base catalysts (oxides: 78–99 %, alumina composites: 52–85 %, zeolites and aluminophosphite zeotypes: 14–90 %) under reflux and autoclave conditions. Furthermore, the Cs-ABW nanozeolite showed catalytic performance comparable to hydrotalcites (92–98 %) and zeolite MgO/Cs,NaY (98 %), the latter conducted using microwave heating. These results suggest that the instant heating technique used here can mimic microwave heating (fast heat transfer and homogenous heating) *via* strong stirring and rapid heating, offering an alternative to the existing catalytic system [58].

4. Conclusion

We performed microwave synthesis of nanoscale Cs-ABW zeolite without using organotemplates. The ABW framework was crystallized within 6 min at much lower temperature (180 °C) and pressure (~20 bar) than the conditions reported before (700–1200 °C, > 1000 bar, 46 h). The nanocrystals were colloidally and thermally stable, and they were active in the cyanoethylation of aliphatic alcohols with acrylonitrile. Furthermore, the cyanoethylation of methanol catalyzed by nanoscale Cs-ABW (100 % conversion) under instant heating was comparable or even more reactive than those catalyzed by other heterogeneous base catalysts (oxides: 78–99 %, alumina composites: 52–85 %, zeolites and aluminophosphite zeotypes: 14–90 %, hydrotalcites: 92–98 %, zeolite MgO/Cs,NaY: 98 %) under microwave, autoclave, or reflux conditions. Thus, this nanoscale zeolite shows great potential in advanced applications, particularly in thin film and catalytic processes.

Declaration of Competing Interest

The authors declare that they have no known competing financial interests or personal relationships that could have appeared to influence the work reported in this paper.

Acknowledgements

The financial support from Fundamental Research Grant Scheme (203/PKIMIA/6711642, 203/PKIMIA/6711461) offered by the Malaysian Ministry of Higher Education is gratefully acknowledged. T.M.A. Ghrear would also like to thank the Fundamental Research Grant Scheme and USM Bridging Fund for the scholarship provided.

Appendix A. Supplementary data

Supplementary material related to this article can be found, in the online version, at doi:https://doi.org/10.1016/j.materresbull.2019.110691.

References

[1] S.M. Al-Jubouri, S.M. Holmes, Chem. Eng. J. 308 (2017) 476–491.
[2] D.Y. Khoo, W.M. Kok, R.R. Mukti, S. Mintova, E.-P. Ng, Solid State Sci. 25 (2013) 63–69.
[3] S. Mintova, J. Grand, V. Valtchev, CR Chim. 19 (2016) 183e191.
[4] V. Valtchev, L. Tosheva, Chem. Rev. 113 (2013) 6734e6760.
[5] S.-F. Wong, H. Awala, A. Vincente, R. Retoux, T.C. Ling, S. Mintova, R.R. Mukti, E.-P. Ng, Microporous Mesoporous Mater. 249 (2017) 105–110.
[6] F. Tong, J. Gong, M. Li, C. Zeng, L. Zhang, Microporous Mesoporous Mater. 213 (2015) 1–7.
[7] G. Majano, E.-P. Ng, L. Lakiss, S. Mintova, Green Chem. 13 (2011) 2435–2440.
[8] L. Tosheva, E.-P. Ng, S. Mintova, M. Holzl, T.H. Metzger, A.M. Doyle, Chem. Mater. 20 (2008) 5721–5726.
[9] W. Shan, T. Yu, B. Wang, J. Hu, Y. Zhang, X. Wang, Y. Tang, Chem. Mater. 18 (2006) 3169–3172.

[10] M. Rahimi, E.-P. Ng, K. Bakhtiari, M. Vinciguerra, H.A. Ahmad, H. Awala, S. Mintova, M. Daghighi, F.B. Rostami, M. de Vries, M.M. Motazacker, M.P. Peppelenbosch, M. Mahmoudi, F. Rezaee, Sci. Rep. 5 (2015) 17259.
[11] A.G. Mohammad S, N.H. Ahmad, K. Goldyn, S. Mintova, T.C. Ling, E.-P. Ng, Mater. Res. Exp. 6 (2019) 025026.
[12] Y. Kamimura, W. Chailittisilp, K. Itabashi, A. Shimojima, T. Okubo, Chem. Asian J. 5 (2010) 2182–2191.
[13] S.-F. Wong, K. Deekamwong, J. Wittayakun, T.C. Ling, O. Muraza, H.L. Lee, F. Adam, E.-P. Ng, Sains Malays. 47 (2018) 337–345.
[14] E.-P. Ng, H. Awala, J.-P. Ghoy, A. Vincente, T.C. Ling, Y.H. Ng, S. Mintova, F. Adam, Mater. Chem. Phys. 159 (2015) 38–45.
[15] H. Awala, J.P. Gilson, R. Retoux, P. Boullay, J.M. Goupil, V. Valtchev, S. Mintova, Nat. Mater. 14 (2015) 447–451.
[16] J. Kecht, B. Mihailova, K. Karaghiosoff, S. Mintova, T. Bein, Langmuir 20 (2004) 5271–5276.
[17] V.P. Valtchev, L. Tosheva, K.N. Bozhilov, Langmuir 21 (2005) 10724–10729.
[18] E.-P. Ng, G.K. Lim, G.-L. Khoo, K.-H. Tan, B.S. Ooi, F. Adam, T.C. Ling, K.-L. Wong, Mater. Chem. Phys. 155 (2015) 30–35.
[19] M. Tsapatsis, T. Okubo, M. Lovallo, M.E. Davis, Mater. Res. Soc. Symp. Proc. 371 (1995) 21–26.
[20] Y. Liu, M. Sun, C.M. Lew, J. Wang, Y. Yan, Adv. Funct. Mater. 18 (2008) 1732–1738.
[21] Y.-W. Cheong, K.-L. Wong, T.C. Ling, E.-P. Ng, Mater. Express 8 (2018) 463–468.
[22] K. Jiao, X. Xu, Z. Lv, J. Song, M. He, H. Gies, Microporous Mesoporous Mater. 225 (2016) 98–104.
[23] T. Kurniawan, O. Muraza, K. Miyake, A.S. Hakeem, Y. Hirota, A.M. Al-Amer, N. Nishiyama, Ind. Eng. Chem. Res. 56 (2017) 4258–4266.
[24] W. Fan, K. Morozumi, R. Kimura, T. Yokoi, T. Okubo, Langmuir 24 (2008) 6952–6958.
[25] E.-P. Ng, L. Delmotte, S. Mintova, Green Chem. 10 (2008) 1043–1048.
[26] E.-P. Ng, S.S. Sekhon, S. Mintova, Chem. Commun. 0 (2009) 1661–1663.
[27] G. Majano, K. Raltchev, A. Vicente, S. Mintova, Nanoscale 7 (2015) 5787–5793.
[28] X. Chen, D. Xi, Q. Sun, N. Wang, Z. Dai, D. Fan, V. Valtchev, J. Yu, Microporous Mesoporous Mater. 234 (2016) 401–408.
[29] S. Mintova, N.H. Olson, V. Valtchev, T. Bein, Science 283 (1999) 958–960.
[30] W. Song, V.H. Grassian, S.C. Larsen, Chem. Commun. (2005) 2951–2953.
[31] E.-P. Ng, D.T.-L. Ng, H. Awala, K.-L. Wong, S. Mintova, Mater. Lett. 132 (2014) 126–129.
[32] S.-F. Wong, K. Deekomwong, J. Wittayakun, T.C. Ling, O. Muraza, F. Adam, E.-P. Ng, Mater. Chem. Phys. 196 (2017) 295–301.
[33] S.A. Gallagher, G.J. McCarthy, Mater. Res. Bull. 12 (1977) 1183–1190.
[34] G.D. Gatta, N. Rotiroti, P.F. Zanazz, M. Rieder, M. Drabek, Z. Weiss, R. Klaska, Am. Mineral. 93 (2008) 988–995.
[35] R. Klaska, O. Jarchow, Naturwiss 60 (1973) 299.
[36] R. Klaska, O. Jarchow, Z. Kristallogr. 142 (1975) 225–238.
[37] K. Yanagisawa, S. Kanahara, M. Nishioka, N. Yamasaki, J. Nucl. Sci. Technol. 21 (1984) 550–558.
[38] J. Yan, C. Zhang, C. Ning, Y. Tang, Y. Zhang, L. Chen, S. Gao, Z. Wang, W. Zhang, J. Ind. Eng. Chem. 25 (2015) 344–351.
[39] Z. Klika, Z. Weiss, M. Mellini, M. Drabek, Appl. Geochem. 21 (2006) 405–418.
[40] M. Mellini, Z. Weiss, M. Rieder, M. Drabek, Eur. J. Mineral. 8 (1996) 1265–1271.
[41] P. Comodi, P.F. Zanazzi, Z. Weiss, M. Rieder, M. Drábek, Am. Mineral. 84 (1999) 325–332.
[42] B.H. Toby, Powder Diffr. 21 (2006) 67–70.
[43] K.I. Rybakov, E.A. Olevsky, E.V. Krikun, J. Am. Ceram. Soc. 96 (2013) 1003–1020.
[44] C.S. Lim, A. Aleksandrovsky, M. Molokeev, A. Oreshonkov, V. Atuchin, Phys. Chem. Chem. Phys. 17 (2015) 19278–19287.
[45] C.S. Lim, A.S. Aleksandrovsky, M.S. Molokeev, A.S. Oreshonkov, V.V. Atuchin, J. Alloys. Compd. 713 (2017) 156–163.
[46] F. Adam, J.N. Appaturi, E.-P. Ng, J. Mol. Catal. A Chem. 386 (2014) 42–48.
[47] E.-P. Ng, J.-Y. Goh, T.C. Ling, R.R. Mukti, Nanoscale Res. Lett. 8 (2013) 120.
[48] T. Kawai, K. Tsutsumi, J. Colloid Interface Sci. 212 (1999) 310–316.
[49] N.N. Golovnev, M.S. Molokeev, S.N. Vereshchagin, V.V. Atuchin, J. Coord. Chem. 68 (2015) 1865–1877.
[50] N.N. Golovnev, M.S. Molokeev, M.K. Lesnikov, V.V. Atuchin, Chem. Phys. Lett. 653 (2016) 54–59.
[51] PubChem database: https://www.ncbi.nlm.nih.gov/pccompound, 2018 (Accessed 20 July 2018).
[52] H. Kabashima, H. Hattori, Catal. Today 44 (1998) 277–283.
[53] P.S. Kumbhar, J. Sanchez-Valente, F. Figueras, Chem. Commun. 0 (1998) 1091.
[54] B.M. Choudary, M.L. Kantam, B. Kavita, Green Chem. 1 (1999) 289–292.
[55] E.-P. Ng, J.-H. Chow, R.R. Mukti, O. Muraza, T.C. Ling, K.-L. Wong, Mater. Chem. Phys. 201 (2017) 78–85.
[56] S. Zamanian, A.N. Kharat, Chin. J. Catal. 35 (2014) 264–269.
[57] H. Abdullahi, K.-L. Wong, G.K. Lim, H. Awala, A. Vicente, T.C. Ling, S. Mintova, E.-P. Ng, Mater. Chem. Phys. 222 (2019) 81–86.
[58] S.-H. Guo, S.-Z. Xing, S. Mao, Y.-R. Gao, W.-L. Chen, Y.-Q. Wang, Tetrahedron Lett. 55 (2014) 6718–6720.